Ferroelectric negative capacitance

Jorge Íñiguez[1,2]*, Pavlo Zubko[3], Igor Luk'yanchuk[4] and Andrés Cano[5,6]

Abstract | The capacitor is a key element of electronic devices and is characterized by positive capacitance. However, a negative capacitance (NC) behaviour may occur in certain cases and implies a local voltage drop opposed to the overall applied bias. Therefore, a local NC response results in voltage enhancement across the rest of the circuit. Within a suitably designed heterostructure, ferroelectrics display such an NC effect, and various ferroelectric-based microelectronic and nanoelectronic devices have been developed, showing improved performance attributed to NC. However, the exact physical nature of the NC response and direct experimental evidence remain elusive or controversial thus far. In this Review, we discuss the physical mechanisms responsible for ferroelectric NC, tackling static and transient NC responses. We examine ferroelectric responses to voltage and charge, as well as ferroelectric switching, and discuss proof-of-concept experiments and possibilities for device implementation. Finally, we highlight different approaches for the optimization of the intrinsic NC response to maximize voltage amplification.

[1]Materials Research and Technology Department, Luxembourg Institute of Science and Technology (LIST), Esch/Alzette, Luxembourg.

[2]Physics and Materials Science Research Unit, University of Luxembourg, Belvaux, Luxembourg.

[3]London Centre for Nanotechnology and Department of Physics and Astronomy, University College London, London, UK.

[4]Laboratory of Condensed Matter Physics, University of Picardie, Amiens, France.

[5]Institut Néel, CNRS & Université Grenoble Alpes, Grenoble, France.

[6]Department of Materials, ETH Zurich, Zurich, Switzerland.

*e-mail: jorge.iniguez@list.lu; p.zubko@ucl.ac.uk; lukyanc@ferroix.net; andres.cano@neel.cnrs.fr

https://doi.org/10.1038/s41578-019-0089-0

The capacitor is one of the most basic components of electronic devices (BOX 1) and is characterized by its capacitance C, which relates the charges $\pm Q$ on the plates of the capacitor to the voltage V between them as $Q = CV$. The capacitance further relates the electrical energy U stored in the capacitor to its charge, $U = Q^2/(2C)$. This electrostatic energy is positive definite[1], and thus the capacitance is a positive quantity. In fact, according to the principle of minimum energy, a capacitor with negative capacitance (NC) would charge spontaneously.

Despite this fundamental constraint, the hypothetical virtues of electronic circuits containing NC components have long attracted the interest of electrical engineers[2–6]. The realization of NC behaviour in ferroelectrics was first proposed by Landauer in 1976 (REF.[7]). Indeed, the appearance of a spontaneous polarization in a ferroelectric slab is reminiscent of the spontaneous charging of a capacitor with NC (BOX 1). Thanks to the landmark works of Bratkovsky and Levanyuk[8,9], today we know that an effective NC response is a hallmark of ferroelectric domain structures with partial screening. The possibility of NC-based voltage amplification, envisioned by Salahuddin and Datta[10], further increased the interest in ferroelectric NC effects[11–14]. In particular, ferroelectric NC can be used to overcome the so-called Boltzmann tyranny that limits the performance of conventional transistors (FIG. 1). This possibility enables ultralow-power nanoelectronic applications with the potential to resolve the energy challenge associated with very-large-scale-integration technologies. The current outburst of activity in the NC field is also related to the emergence of new HfO_2-based ferroelectric materials[15–18], which outperform traditional perovskite oxides in terms of complementary metal-oxide-semiconductor compatibility. Ferroelectric NC is currently explored not only in proof-of-principle experiments and modelling but also for materials optimization and device implementation. Thus, this field gathers often distant research communities, including physicists, materials scientists and electrical engineers. Therefore, fundamental concepts, including terminology, need to be clarified, and a common ground for NC research needs to be established.

Global versus local capacitance

The fundamental principle of minimum energy states that capacitance cannot be negative. This principle is global and applies to the capacitor as a whole; however, it allows considerable flexibility at the local level. An inhomogeneous capacitor with two dielectrics between the plates can be modelled as two capacitors in series C_1 and C_2 (FIG. 1a). The overall capacitance is then $C = (C_1^{-1} + C_2^{-1})^{-1}$, which needs to be positive owing to thermodynamic stability. However, this relation is also true if one of the local effective capacitances, for example, C_1, is negative, as long as the condition $C \geq 0$ is fulfilled.

In this scenario, the application of an external voltage V results in $V_{int} = V(1 + C_2/C_1)^{-1}$ at the interface between the two dielectrics, such that $V_{int}/V > 1$ if $C_1 < 0$. That is, NC of one part of the system enables amplification of the voltage at the interface (FIG. 1b). Contrary to the usual decrease in the overall capacitance when a regular (positive) capacitance is added in series, the addition of

NC increases the total capacitance of the system. This capacitance boost is one of the hallmarks of NC.

The definition of capacitance as $C = Q/V$ is valid only for a linear dielectric capacitor, in which such capacitance coincides with the differential capacitance $C = dQ/dV$. The differential capacitance is the physically relevant quantity for nonlinear dielectrics such as ferroelectrics (BOX 2). Another important consideration pertains to the capacitance and its relation to the dielectric permittivity. A positive global capacitance implies that the application of an external electric field E_{ext} is followed by the displacement field D (that is, the charge) such that $\Delta D/\Delta E_{ext} > 0$. The permittivity $\varepsilon(\boldsymbol{r}) = \varepsilon_0^{-1}\delta D(\boldsymbol{r})/\delta E(\boldsymbol{r})$ at point $\boldsymbol{r}$ gives the change in displacement field $D(\boldsymbol{r})$ in response to a variation in the local electric field $E(\boldsymbol{r})$ (ε_0 is the vacuum permittivity). Owing to the long-range character of Coulomb interactions, $\varepsilon(\boldsymbol{r})$ depends on the response of the material in regions distant from $\boldsymbol{r}$, which makes its behaviour not obvious. In particular, nothing prevents it from being locally negative, such that the change in $D(\boldsymbol{r})$ opposes the change in $E(\boldsymbol{r})$. By contrast, a change in $D(\boldsymbol{r})$ is expected to follow the change in the external electric field E_{ext}, resulting in a positive $\Delta D(\boldsymbol{r})/\Delta E_{ext}$. The local capacitance, or capacitance of part of a system, is essentially equal to the local $\varepsilon(\boldsymbol{r})$, except for geometric factors, and therefore can be negative. Note that this definition of a 'local' capacitance based on $\varepsilon(\boldsymbol{r})$ is not standard; the usual definition of capacitance pertains to a whole system and is related to the total effective ε. Finally, note that the local permittivity is a static equilibrium quantity and not directly related to the refractive index at optical frequencies. Therefore, a negative local permittivity does not automatically imply an anomalous refractive index.

Box 1 | Capacitance and ferroelectrics

Capacitance

The capacitance C refers to the mutual capacitance between two conductors (in contrast to the self-capacitance of an isolated conductor). Ideally, C is entirely determined by the geometry of the capacitor and the dielectric response of the medium between the plates. For the parallel-plate linear capacitor (see the figure, panel **a**), $C = \varepsilon A/d$, where A is the area of the plates, d is the distance between them and ε is the permittivity of the linear dielectric medium (from Maxwell's equations). Capacitors are usually represented as shown in the figure, panel **b**; a positive applied voltage ($V > 0$) charges the plates ($Q > 0$), creating an electric field ($E = V/d$, arrows shown in the figure, panel **b**) in the dielectric.

Ferroelectrics

Ferroelectric materials undergo a transformation from a nonpolar paraelectric phase to a phase with switchable, spontaneous electric polarization P, which can be inhomogeneous in a multidomain state. According to the Landau theory of phase transitions, polarization is taken as the order parameter; the corresponding free energy is shown in the figure, panel **c**. This energy can be obtained from first principles, and its functional derivative defines the constitutive equation $P(E)$ (or $D(E)$, where D is the displacement field) of the ferroelectric. This equation, together with the Maxwell–Faraday equation and Gauss' law (that is, Maxwell's equations), determines the electric response of the system and therefore the corresponding capacitance of a ferroelectric capacitor.

Depolarizing fields

Depolarizing fields appear when there is a non-vanishing polarization bound charge $\rho_{bound} = -\nabla \cdot P$. These fields (black arrows shown in the figure, panel **d**, representing an infinite ferroelectric slab) unavoidably occur in ferroelectrics if the spontaneous polarization is normal to the sample surfaces, contributing to the energy of the system.

Domains and domain walls

A ferroelectric domain is a region in which the electric polarization can be considered as approximately uniform. In a multidomain state (see the figure, panel **e**), polarization of different domains is oriented along different directions, and the domains are separated by domain walls. The domain wall self-energy increases the overall energy; however, the energy of the depolarizing or stray fields (black arrows shown in the figure, panel **e**) decreases as domains become narrower. This antagonism determines the spontaneous occurrence of domains.

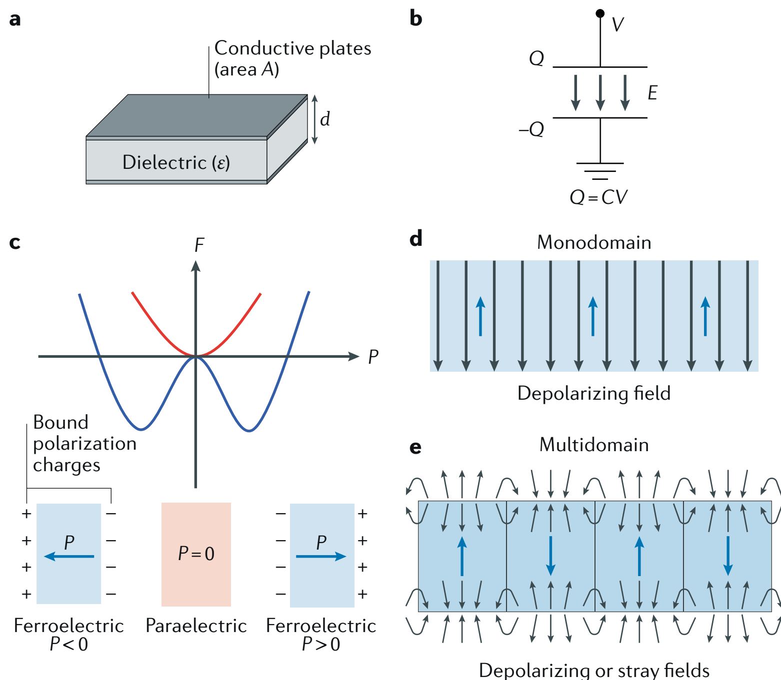

Ferroelectric NC

Response to voltage and charge. The key to obtaining NC is to exploit an inherent instability that directly couples to the electric field. A variety of systems with such instabilities have been proposed[19–21]; however, the best-studied instability is the ferroelectric transition in ferroelectric materials (BOXES 1,2).

Let us examine the behaviour of a ferroelectric capacitor[7] assuming a uniform polarization within the ferroelectric (that is, there are no domains). In a typical setup, the capacitor is driven by a voltage source V, and the charge on the capacitor plates Q is measured by integrating the displacement current flowing through the circuit. In the ferroelectric phase, the constitutive $Q(V)$ relation becomes a multi-valued S-shaped function (BOX 2) with a negative-slope segment that would enable NC. However, this segment is unstable, and consequently, for any applied voltage within this multi-valued region, the actual charge of an adiabatic voltage-driven process corresponds to one of the two branches with positive slope, that is, positive capacitance. This behaviour results in a hysteresis, usually observed in the measured $Q(V)$ and $C(V)$ (BOX 2).

By contrast, if the ferroelectric capacitor is driven by a charge, the multi-valued S-shaped $Q(V)$ function is flipped, becoming an N-shaped $V(Q)$ relation (BOX 2). The N-shaped $V(Q)$ curve is a single-valued function, which also includes the point ($V = 0$, $Q = 0$) and a negative-slope region around it. Thus, by controlling the charge Q, the NC behaviour becomes accessible.

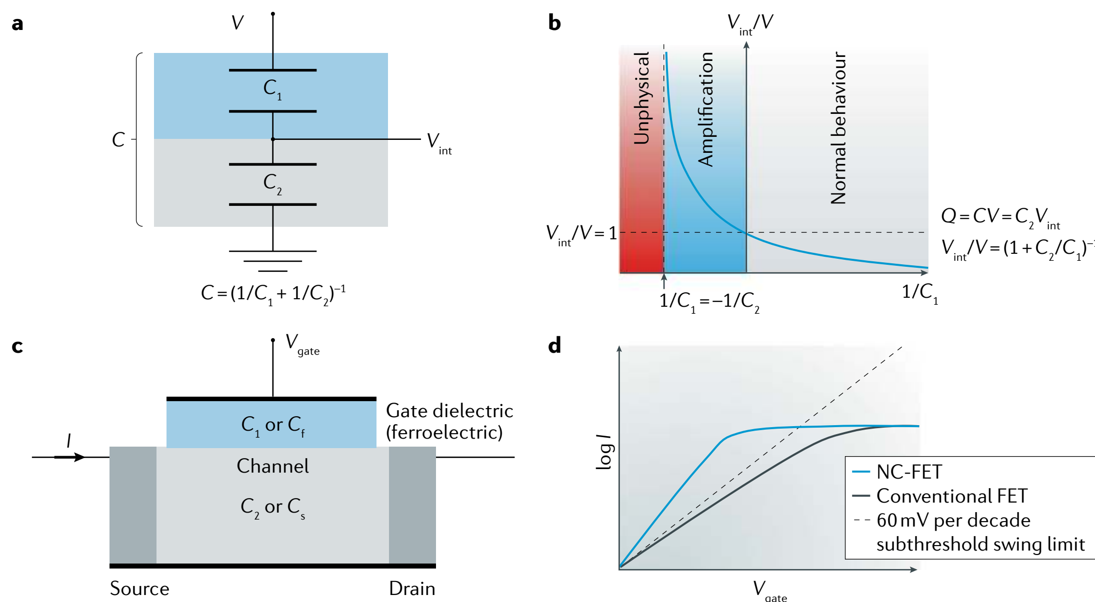

Fig. 1 | **Negative capacitance for voltage amplification. a** | Schematic of a composite dielectric, modelled as two capacitors, C_1 and C_2, in series. V_{int} is the voltage at the interface between C_1 and C_2, which can be written as a function of the external voltage V: $V_{int} = V/(1 + C_2/C_1)$. **b** | The voltage ratio V_{int}/V as a function of C_1^{-1} for a fixed positive value of C_2^{-1} shows the allowed regime of negative capacitance (NC) that leads to voltage enhancement. **c** | Schematic of a field-effect transistor (FET) showing the effective inhomogeneous capacitance for the gate dielectric (C_1) and channel (C_2 or series capacitance C_s). In ferroelectric FETs, the gate dielectric is replaced by a ferroelectric that can operate in its NC regime (C_1 or ferroelectric capacitance C_f). **d** | In NC-FETs, for $C_f < 0$, the theoretical limit (Boltzmann tyranny) for the subthreshold swing can be overcome. I, current; Q, electric charge; V_{gate}, gate potential.

Incipient ferroelectricity. A simple way of controlling charge is to connect an ideal ferroelectric capacitor in series with a regular dielectric capacitor[10]. For example, in the setup discussed above, C_1 can be understood as the ferroelectric capacitance (C_f), and C_2 as the series capacitance (C_s) (FIG. 1c,d). The two capacitors must have the same charge on their plates and thus are electrostatically coupled. The accessible values of charge can then be graphically deduced (BOX 2). For small C_s values (that is, for a capacitor made of a dielectrically stiff material), the effect of the series capacitance is to suppress the spontaneous polarization in the ferroelectric and thus to stabilize the paraelectric state even if the ferroelectric is below its nominal transition temperature (FIG. 2). In this region, the system becomes an incipient ferroelectric, and NC is realized in the ferroelectric stack (FIG. 3a)[22]. The internal voltage drop in the ferroelectric is opposed to the overall external bias, which automatically leads to an increase in voltage at the interface.

Conceptually, the effect of the series capacitor is identical to that of the well-studied ‘dead layers’ or finite screening lengths at the metal–ferroelectric interfaces in a ferroelectric capacitor[8,23–25], at the dielectric layers in ferroelectric–dielectric superlattices and multilayers[26,27] and in the semiconductor channel of a field-effect transistor (FET) (FIG. 1). Thus, these systems display NC in the appropriate temperature range and can serve as model systems for the experimental and theoretical investigation of NC. Importantly, although the experimentally controlled parameter is often the total applied voltage, the state of the ferroelectric component is determined by the charge on the corresponding series capacitance C_s, allowing effective charge control.

The incipient ferroelectric NC regime is physically realized by the incomplete screening of the polarization bound charges that would produce a depolarizing field (BOX 1)[22]. The emergence of this field implies an energy penalty (and thus additional stiffness), which, together with the energy cost of charging the coupled series capacitor, shifts the homogeneous ferroelectric instability down to $T_{\uparrow\uparrow}$, which is below the nominal transition temperature T_0. Accordingly, the paraelectric state ($V = 0$, $Q = 0$) is preserved below T_0 until the eventual transition point is reached (FIG. 2).

The different states of the ferroelectric are accessible by changing the temperature (FIG. 2). Although the NC regime also continues below $T_{\uparrow\uparrow}$ into the homogeneous ferroelectric phase, it may be accompanied by a hysteresis, which is undesirable for low-power applications. Therefore, for devices, the temperature range of interest corresponds to the incipient ferroelectric regime $T_{\uparrow\uparrow} < T < T_0$. The maximum voltage amplification at the interface occurs at $T_{\uparrow\uparrow}$ (REF.[22]), at which the slope of the $Q(V_f)$ curve at $V_f = 0$ is $-C_s$, that is, the total capacitance of the system diverges — this condition is usually referred to as capacitance matching (FIG. 2). This occurs at a specific temperature for a specific value of C_s, which presents a challenge for the design of NC devices in which such a non-ferroelectric capacitance exhibits large variations; for example, in NC-FETs, in which the channel is driven between depletion and inversion. Therefore, optimization of capacitance matching in NC devices is an active area of research[20,28]. Finally, as we

Box 2 | **Ferroelectric response**

The intrinsic response of a ferroelectric to an applied voltage V (or an applied electric field $E=V/d$, where d is defined in panel **a** of the figure in (BOX 1) is fundamentally different from the response to an external 'capacitive' charge Q at the interfaces of the ferroelectric (equivalent to constraining the displacement field $D=Q/A$, where A is defined in panel **a** of the figure in (BOX 1)). Accordingly, the constitutive relations $Q(V)$ (or $D(E)$) and $V(Q)$ (or $E(D)$) (see the figure, panels **a** and **b**) show different behaviours. These constitutive relations determine the (nonlinear) differential capacitance $C(V_0)=dQ/dV$, defined at the operating voltage V_0, and its inverse function $C^{-1}(Q_0)=dV/dQ$, defined at the operating charge Q_0 (see the figure, panels **c** and **d**). The multi-valued character of the constitutive equation $Q(V)$ in the negative capacitance (NC) region prevents the stabilization of the NC state (dashed lines in the blue $Q(V)$ curve shown in the figure, panel **a**) by controlling V. By contrast, the constitutive equation $V(Q)$ becomes a single-valued function, which enables the physical realization of the (static) NC regime by controlling the charge Q.

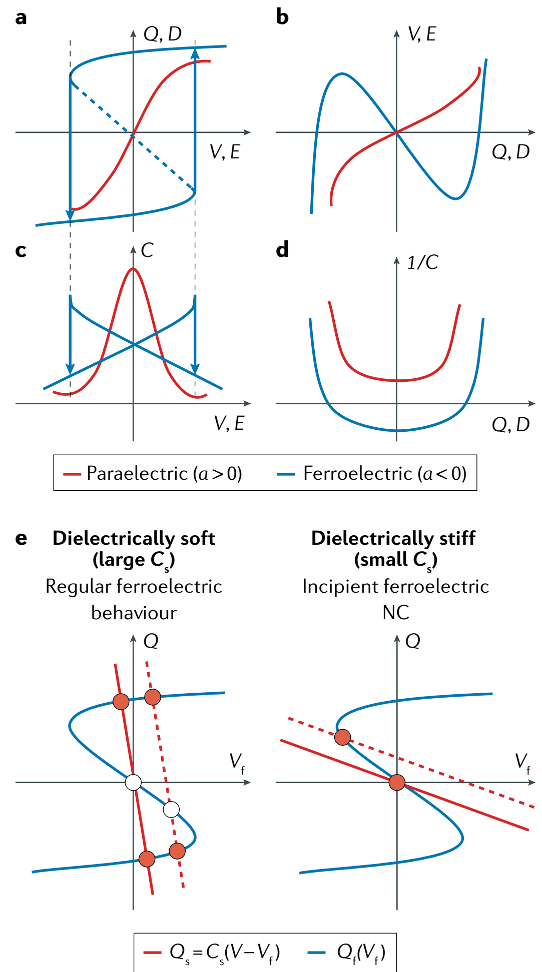

Key equations

The simplest Landau free energy F for a ferroelectric and the corresponding equilibrium constitutive equation are

$$F=\frac{a}{2}P^2+\frac{b}{4}P^4-EP\rightarrow aP+bP^3=E \qquad (8)$$

where P is the electric polarization. The change from $a>0$ (paraelectric) to $a<0$ (ferroelectric) marks the (second order) transition. For a parallel-plate capacitor geometry (BOX 1), $P(D)=D-\varepsilon_0\,E=(\frac{Q}{A}-\varepsilon_0\frac{V}{d})$, where ε_0 is the vacuum permittivity. Therefore, the equilibrium condition can be rewritten as

$$Q+\frac{b}{aA^2}(Q-C_0V)^3=C_f^{(0)}V \qquad (9)$$

where $C_0=\varepsilon_0\frac{A}{d}$ is the capacitance that would be associated with an empty capacitor, while $C_f^{(0)}=(1+\frac{1}{\varepsilon_0 a})C_0$ is the capacitance of the ferroelectric at zero applied voltage. This equation can be used to derive the voltage-control ($Q(V)$, see the figure, panel **a**) or charge-control ($V(Q)$, see the figure, panel **b**) constitutive equations.

Series capacitors

Two capacitors in series have the same charge. Thus, for an externally applied bias $V=V_f+V_s$, the charge of a ferroelectric capacitor (C_f) in series with a regular capacitor (C_s) is given by the points of intersection between the ferroelectric S-shaped $Q_f(V_f)$ curve and the load line of the dielectric $Q_s=C_s(V-V_f)$ (see the figure, panel **e**). For large C_s (dielectrically soft series capacitor), three possible solutions at small V exist: two (meta)stable solutions (solid circles in panel **e**) and one unstable solution (open circle in the figure, panel **e**). The (meta)stable solutions trace the typical hysteresis loop of a ferroelectric as a function of V. By contrast, for sufficiently small C_s (dielectrically stiff series capacitor), the only solution at $V=0$ is $Q=0$. Upon application of a positive V, this solution shifts to negative V_f, resulting in a negative differential capacitance $C_f=dQ_f/dV_f<0$, which corresponds to the incipient ferroelectric NC regime.

cool down below $T_{\uparrow\uparrow}$, a single-domain ferroelectric polarization develops, causing an increase in C_f, which may eventually become positive (FIG. 2).

Multidomain ferroelectricity. The assumption that the state of the ferroelectric is perfectly uniform holds true in the paraelectric and incipient ferroelectric regimes. However, the appearance of ferroelectricity generally implies the emergence of ferroelectric domains. The reason is again related to the depolarizing field: compared with the single-domain state, multidomain ferroelectricity confines the depolarizing field to distances on the order of the size of the domains and thus drastically reduces its energy (BOX 1). Therefore, the multidomain state tends to emerge at a temperature $T_{\uparrow\downarrow}$, which is closer to the nominal transition temperature ($T_{\uparrow\downarrow}\lesssim T_0$) than to the theoretical single-domain instability ($T_{\uparrow\downarrow}>T_{\uparrow\uparrow}$)[22,29] (FIG. 2). Consequently, multidomain physics becomes essential for the interpretation and implementation of ferroelectric NC beyond the incipient ferroelectric regime.

A simple and illustrative case is a 180° Kittel domain pattern (FIG. 3b). In a 180° Kittel domain pattern, the widths of the up and down domains are equal ($w_\uparrow=w_\downarrow$)

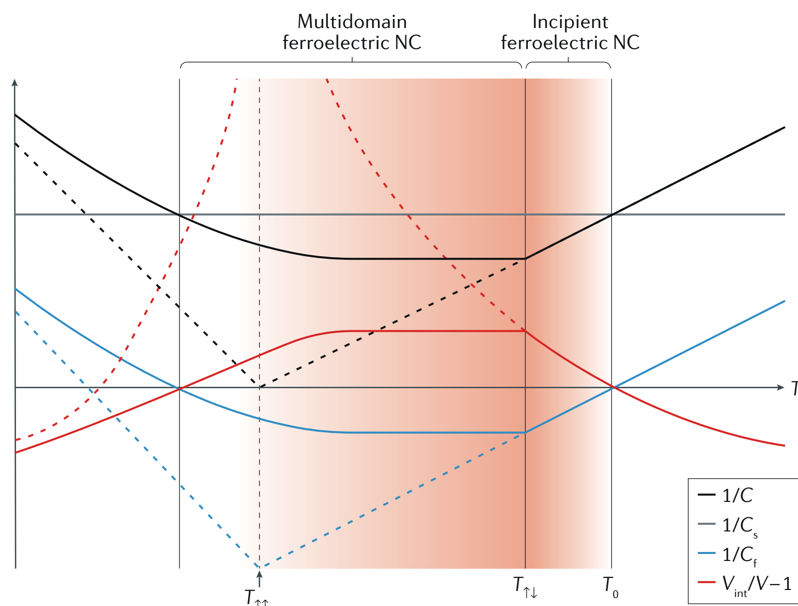

Fig. 2 | **Negative capacitance regimes.** The temperature (T) dependence of the capacitance C (black curve) of a capacitor stack is shown. C_f corresponds to a ferroelectric and is strongly T-dependent (blue curve); C_s (grey line) represents a dielectric and is assumed to be constant. At high T, the behaviour of the stack is normal, with C_s and C_f greater than 0. Below the nominal transition temperature T_0, the ferroelectric develops an intrinsic instability ($C_f < 0$), but the presence of the dielectric prevents the occurrence of a phase transition, leading to negative capacitance (NC) behaviour in the incipient ferroelectric regime. The ferroelectric then transforms into a multidomain state at $T = T_{\uparrow\downarrow}$. Typically, C_f^{-1} increases at this point, reflecting the fact that the ferroelectric becomes less responsive owing to the energy cost of moving domain walls. However, for $T < T_{\uparrow\downarrow}$, and as long as C_f^{-1} remains negative, the ferroelectric multidomain state presents an NC response. If the formation of ferroelectric domains is precluded, C_f^{-1} follows the dashed blue line and increases below a temperature $T_{\uparrow\uparrow}$, at which the transition to a single-domain ferroelectric state occurs. The voltage amplification ratio V_{int}/V is at its maximum for the smallest C_f^{-1}, which typically coincides with $T_{\uparrow\downarrow}$ (solid red line), unless the formation of domains is precluded and the ferroelectric transition occurs at $T_{\uparrow\uparrow}$ (at which the amplification would become infinite; dashed red and black lines). Of note, the multidomain NC regime can in principle extend down to 0 K. Similarly, $T_{\uparrow\uparrow}$ can also be negative, such that the transition to a single ferroelectric domain never occurs; there is no fundamental reason preventing such behaviours.

in the absence of external bias, which leads to the creation of macroscopically charge-neutral interfaces. In the presence of a bias, the domain walls are displaced, which causes the expansion (or shrinking) of the domains that are aligned with (or against) the corresponding external field, such that the external charge is matched through the imbalance $u = (w_\uparrow - w_\downarrow)/2 \neq 0$. If the inhomogeneous stray fields are neglected, and in the absence of any pinning, the domain walls have no obstacle to perfectly screen the charge. This response is equivalent to having infinite capacitance (FIG. 3b). However, in real systems, the stray fields cannot be neglected, because their associated energy changes when the system reacts to the bias. These energy changes can be calculated in the different limits of the Kittel model[8,9,30], demonstrating that an additional increase in the imbalance magnitude $|u|$ reduces the overall energy. Therefore, the multidomain state overscreens the external charge, which then leads to an NC behaviour (FIG. 3c).

The origin of overscreening can be explained by introducing universal symmetry arguments[31]. In the multidomain state (FIG. 4a), the change in the free energy of the ferroelectric due to its net polarization can be written as

$$F \approx \frac{1}{\mathcal{C}}\left(\frac{1}{2}\kappa q^2 + Qq\right) \tag{1}$$

where $\mathcal{C}$ and κ are material-dependent constants, Q is the external capacitive charge brought to the interfaces of the ferroelectric by the applied bias and, in the simplest case, the polarization bound charge q can be taken as $q = (u/w)P_0A$, in which P_0 is the spontaneous polarization of the domains, A is the interfacial area, $w = (w_\uparrow + w_\downarrow)/2$ is the average domain width and u is the imbalance, as defined above. The energy is then minimized for

$$q = -Q/\kappa \tag{2}$$

Here, only one degree of freedom of the multidomain state is considered, thus implicitly ignoring inhomogeneous stray fields. The case of perfect compensation mentioned above (that is, $q = -Q$) is then obtained for $\kappa = 1$ (FIG. 4b).

However, the response of a multidomain state to the external charge Q involves additional degrees of freedom. These can be described by bound-charge density waves compatible with the multidomain periodicity and that effectively incorporate the aforementioned depolarizing field effects (FIG. 4). If q' denotes the wave sketched in FIG. 4c, which is polar and thus contributes to the linear dielectric response of the multidomain state, a more complete expression for the energy F can be written as

$$F \approx \frac{1}{\mathcal{C}}\left(\frac{1}{2}\kappa q^2 + \frac{1}{2}\kappa' q'^2 + \delta q q' + Qq\right) \tag{3}$$

The key additional feature is the bilinear coupling δ between q and q', which is specific to and universally present in multidomain states. This coupling is responsible for the coordinated response of q and q'. In the particular case of the q'-wave (FIG. 4c), δ accounts for the fact that the polarizability of the domain wall regions is different (presumably much larger) from that of the domains. Thus, δ can be expected to be strong.

Minimization of equation 3 over q' yields

$$F \approx \frac{1}{\mathcal{C}}\left(\frac{1}{2}\kappa_* q^2 + Qq\right) \tag{4}$$

where $\kappa_* = \kappa - \delta^2/(2\kappa')$. Compared with equation 1, the additional degrees of freedom that are active in the multidomain state produce an effective renormalization of the polarization stiffness $\kappa \rightarrow \kappa_* < \kappa$, which softens the system. Note that κ_* must be positive so that the net polarization of the multidomain state is zero in the absence of external bias. However, the renormalized stiffness can become very small; in particular, we can have $\kappa_* < 1$, and therefore the relation

$$|q| = |Q|/\kappa_* > |Q| \tag{5}$$

holds true in the corresponding equilibrium state (that is, after minimization over q). This results in the overscreening of the external charge Q and thus NC behaviour (FIG. 3c).

These relations can be considered universal: ferroelectric multidomain states always present inhomogeneous, symmetry-wise polar charge modulations that couple bilinearly with the homogeneous charge (FIG. 4). These inhomogeneous charge waves always result in an enhanced response, which is essentially unconstrained and typically leads to NC behaviour.

The case described above, in which the chosen q' (FIG. 4c) highlights the different polarizabilities of domains and domain walls, is reminiscent of the NC mechanism found in $PbTiO_3/SrTiO_3$ superlattices[32,33] by second-principles atomistic simulations (domain walls in a high-energy state are very polarizable). By contrast, Bratkovsky and Levanyuk obtained an NC effect from a simple Kittel model, in which the enhanced response is associated with changes in stray fields around the walls[8] (the $-\delta^2/(2\kappa')$ correction roughly corresponds to the inhomogeneous contribution to the computed stiffness). Moreover, an analytical expression for the effective negative permittivity of the ferroelectric layer for a ferroelectric–dielectric superlattice model can be derived in terms of the intrinsic dielectric properties of the individual materials[30], assuming the ferroelectric to be in an idealized multidomain configuration. This analytical result[30] enables further analysis of the conditions leading to overscreening and NC[32,34]. Similarly, the NC response of a model two-domain state, stabilized in a cylindrical ferroelectric nanocapacitor, has also been recently discussed[35].

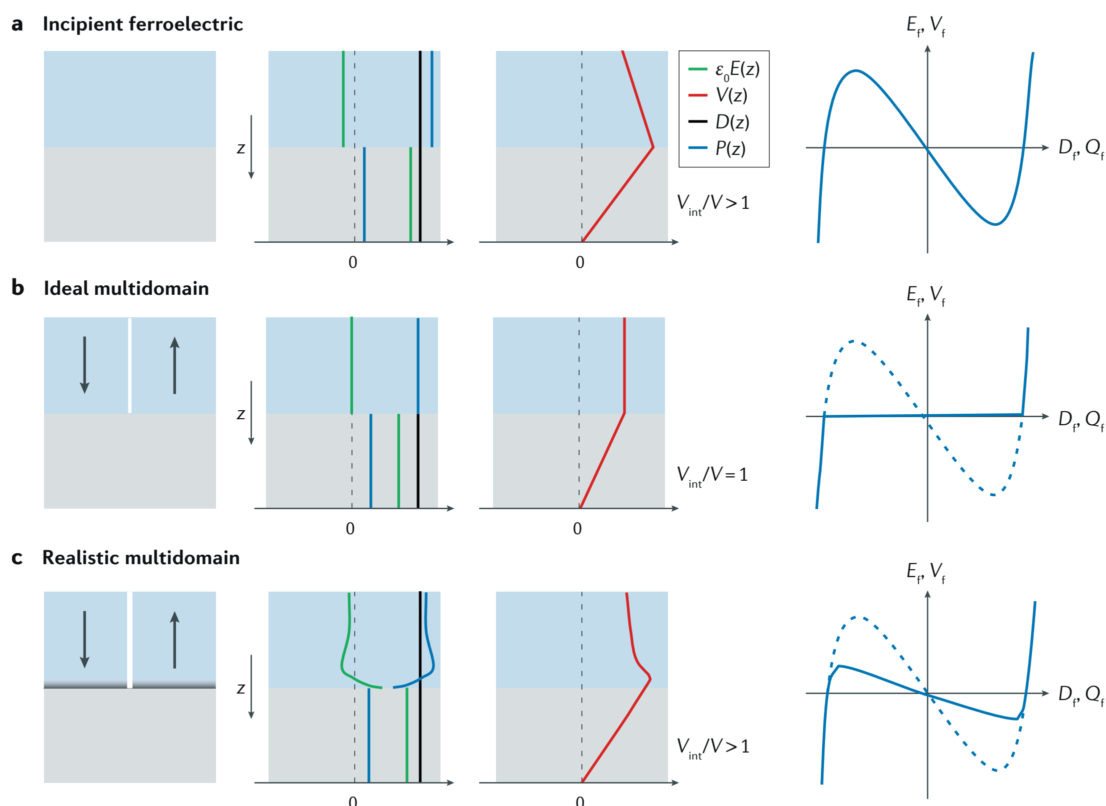

Fig. 3 | **Overscreening and voltage amplification.** An incipient ferroelectric state, a multidomain ferroelectric state with ideal response and a realistic multidomain state are shown for a ferroelectric (blue)–dielectric (grey) stack. Stacks on the left show the equilibrium state at zero applied bias; stacks in the middle show the variation of the polarization $P(z)$ (blue lines), displacement $D(z)$ (black lines) and electric $\epsilon_0E(z)$ (green lines) fields along the capacitor stack for $D(z)=D>0$ by application of an external bias $V>0$; and stacks on the right illustrate the evolution of the potential $V(z)$ (red lines) for that same external bias V (assuming $V(z)=0$ at the bottom of the stack, such that the voltage at the interface $V_{int}=V_s$, and $V_f=V-V_{int}$). The curves representing the constitutive equations of the ferroelectric capacitors are shown for the charge-control scenario. It is assumed that no free carriers exist in the system, such that $D(z)=P(z)+\epsilon_0E(z)=D$ for all z. Imposing $D_f=D$ is equivalent to imposing a charge $Q_f=A_fD_f$ at the dielectric–ferroelectric interface; this control parameter fully determines the electric field (E_f) and voltage drop ($V_f=d_fE_f$) in the ferroelectric, as given by the constitutive equation. **a** | In the incipient ferroelectric case, a positive D_f results in a negative electric field ($\epsilon_0E_f<0$) or, equivalently, in an induced polarization charge that exceeds the external charge ($P_f>D_f=D$), leading to an anomalous overscreening of the external charge in the ferroelectric and an enhanced voltage drop in the dielectric. **b** | In the ideal multidomain case, the domain walls move to exactly compensate the external charge ($P_f=D_f=D$), which corresponds to a $P_f(D_f)$ curve that is flat around $D_f=0$, leading to perfect screening and no amplification. **c** | In the more realistic multidomain case, the additional energy gains result in an overscreening of the external charge and thus negative capacitance (NC) behaviour. Typically, the NC response is not as strong as in the incipient ferroelectric regime (dashed lines in the equation of the state) but is still present.

The physical mechanisms dominating the NC effect may be different in different systems or models; however, a general picture emerges: a ferroelectric multidomain state has the ability (and tendency) to over-respond to an applied charge. This behaviour is the core of multidomain ferroelectric NC.

Ferroelectric switching and transient NC. The NC behaviour discussed so far refers to the purely static response, and it is tacitly assumed that the system is able to adiabatically follow the changes in the applied voltage. However, the ferroelectric response can also enable a temporary reduction in the corresponding voltage $V(t)$ by increasing the charge $Q(t)$ as a function of time t during ferroelectric switching. This behaviour has long been discussed in the literature[7,36] and has recently been called transient NC[37–41].

The intrinsic ferroelectric switching dynamics are typically too fast to be observed in standard experiments; therefore, studies of transient NC have focused on slowing down the delivery of screening charge by connecting the ferroelectric capacitor to a series resistance. Nevertheless, the possibility of observing non-equilibrium NC during fast polarization switching has also been discussed[36].

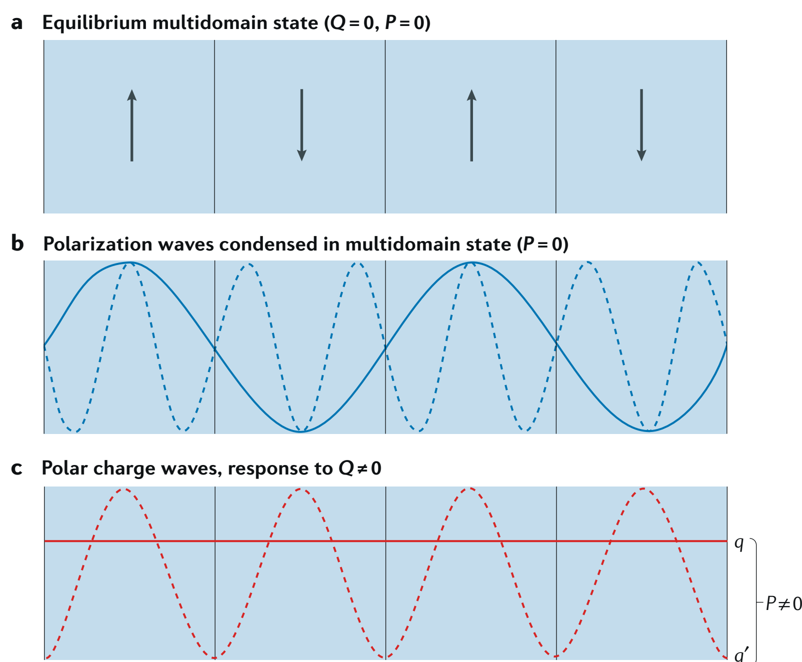

Fig. 4 | **Multidomain state response. a** | Schematic of a multidomain ferroelectric state with an equilibrium configuration that corresponds to zero macroscopic polarization ($P=0$) in the absence of an external charge ($Q=0$). **b** | The multidomain state can be viewed as a superposition of charge waves with no associated net polarization. **c** | The linear dielectric response of a multidomain state is complex; in addition to the uniform response (with the amplitude q), it also involves undulating charge waves (q'). In the paraelectric state, the q'-wave is nonpolar: positive local dipoles cancel with symmetry-equivalent negative dipoles, occurring in other regions of the material, resulting in no macroscopic polarization. Once the multidomain state is condensed, the q'-wave acquires a polar character: the polar distortions in the domain wall regions add up and do not exactly cancel with the distortions in the intra-domain regions. The particular q'-wave shown here is a representative of an infinite series of inhomogeneous charge modulations that become polar in the multidomain state and thus contribute to the linear dielectric response of the system. These modulations are the key to overscreening and to the NC response in a multidomain state.

Conceptually, the simplest ferroelectric switching is the so-called homogeneous or domainless switching, during which the ferroelectric stays in a single-domain state across the whole sample. This hypothetical switching has been extensively discussed in the literature[42–45], and it is believed to be observable only under very special conditions, at which domain formation is energetically or kinetically suppressed, for example, in ultrathin films very close to the Curie point[44] or on ultrafast timescales[45]. In all other cases, switching proceeds by usual domain nucleation and growth[43], and, therefore, the question remains whether transient NC is possible during domain-mediated switching[13].

Indeed, all experimentally reported signatures of transient NC are accompanied by a strong hysteresis, which is characteristic of domain-mediated switching. Such switching involves states in which the energy exhibits a negative curvature and thus is expected to exhibit transient NC during the run-away stage that follows the clearing of the activation barrier. Therefore, both the nucleation and growth of domains with reversed polarization can in principle contribute to transient NC. In reverse-domain nucleation, an energy barrier needs to be overcome for the formation of charged domain wall sections that generate strong electric fields. Domain growth then involves an energy penalty to increase the domain wall area, until the reversed domains start to coalesce. Thus, explicit consideration of the energies associated with domain nucleation and growth is crucial for understanding the experimental observations and for addressing the question of whether the observed voltage reduction can be directly mapped to an effective negative curvature of the free energy[37,39] or whether it might be an artefact typical of complex nonlinear systems[46–48].

Simulations of ferroelectric switching have confirmed that transient NC can be obtained during the process of domain nucleation and growth, but it eventually disappears at the stage of domain coalescence[40]. However, ferroelectric switching is difficult to control owing to its complex stochastic nature in macroscopic and mesoscopic systems. By contrast, in nanoscale devices with dimensions on the order of the characteristic size of the nucleating domains[49], reversal and growth of only one ferroelectric domain can be realized, resulting in controlled transient NC and in static NC in the charge-driven case.

Simulations of ferroelectric switching are usually based on the time-dependent Ginzburg–Landau model[40,41,48,50–52]. For homogeneous domainless switching, the polarization dynamics can be described by the Landau–Khalatnikov dissipative equation

$$\gamma\dot{P}(t) = -aP(t) - bP^3(t) + V(t)/d \tag{6}$$

which is the dynamical extension of the constitutive relation (BOX 2). However, in the more realistic case of domain-mediated switching, equation 6 has to be supplemented with spatial gradient terms and (long-range) dipolar forces. In an ideal ferroelectric capacitor, the

dissipative, time-dependent term on the left-hand side sets the characteristic timescale for the intrinsic relaxational dynamics of the polarization. However, within a circuit, the time-dependent term also includes any external series resistance, which slows down the delivery of the screening charge and, as a result, the switching process itself; indeed, if the ferroelectric polarization were to switch more rapidly, the large mismatch between the polarization and screening charge would lead to a large depolarizing field, which would reduce polarization. Therefore, the internal polarization dynamics follow the dynamics of the screening charge, maintaining a small mismatch between Q/A and P, as dictated by the appropriate (single-domain or multidomain) static S-shaped curve. The charge could be delivered arbitrarily slowly and thus the NC region could, in principle, be probed in a quasi-static way[7]. Therefore, the transient and static effects have the same physical origin, and the difference is related to practical aspects of accessing the NC regime. In a typical transient measurement, the charge is dynamically controlled by the application of voltage. The start and end points of the switching process then correspond to positive energy curvature, and, therefore, voltage amplification cannot be achieved in a static sense.

A wide range of phenomena resulting in non-monotonic transients can give rise to negative values of the measured effective capacitance, as is well documented in semiconductors[53,54]. Ferroelectrics have a semiconducting nature, and thus some of these processes are likely to also occur in ferroelectric systems. Therefore, great care must be taken in distinguishing these effects and inductance-like behaviour (which has a very different frequency dependence) from the ferroelectric NC discussed here.

Experimental evidence of NC

Experimental work on ferroelectric NC can be loosely divided into proof-of-concept experiments and device-implementation attempts. In proof-of-concept work, evidence for NC behaviour has usually been sought by examining the NC response resulting from adding a ferroelectric layer in series with a dielectric. More applied work has focused on realizing the predicted subthreshold swing reduction in transistor devices with ferroelectric gates. Both approaches primarily address static NC behaviour. Attempts to observe the transient effect have focused on the direct measurement of the voltage drop across the ferroelectric during the application of an external bias. These experiments require the ferroelectric capacitor to be isolated and externally accessible, which can be achieved by introducing internal metallization nodes in the transistor stacks or by connecting the ferroelectric capacitors to external metal-oxide-semiconductor FETs (MOSFETs), FinFETs and simple electronic components such as resistors and capacitors.

Proof of concept. The first connection between experiments and NC was made by Bratkovsky and Levanyuk[9], who used experimental data on high-quality ultrathin $SrRuO_3/BaTiO_3/SrRuO_3$ capacitors[55] and a theoretical estimate for the metallic screening length to re-plot the hysteresis curves as a function of the actual voltage drop across the ferroelectric, that is, disentangled from the interfacial drop. The resulting curves display sections with negative slopes (FIG. 5a), attributed to multidomain NC. Essentially equivalent conclusions were reached using data on similar capacitors, for which the involvement of domains was explicitly confirmed, in combination with density functional theory (DFT)-based calculations of the interfacial screening lengths[56]. However, in these approaches, evidence for NC relies on assumed values for the interface capacitance, which is difficult to experimentally control or determine in a self-consistent way. Therefore, the majority of fundamental studies have focused on ferroelectric–dielectric heterostructures, with which the identification of depolarizing field effects is more straightforward.

In the first work representative of such studies, the capacitance of a $SrTiO_3$ layer was compared with that of a $Pb(Zr, Ti)O_3/SrTiO_3$ bilayer[57]. Depositing a ferroelectric layer on top of $SrTiO_3$ results in a structure that, within a certain temperature range, has a larger capacitance than that of the $SrTiO_3$ layer alone (FIG. 5b). Similar capacitance enhancements were later reported in $BaTiO_3/SrTiO_3$ capacitors[58], $(Ba, Sr)TiO_3/LaAlO_3$ superlattices[59] and $BaTiO_3/Al_2O_3$ capacitors[60,61]. Although these studies address static NC behaviour, time dependence still plays an important role because capacitance measurements are usually carried out using AC methods and are further complicated by the dynamic effects of charge trapping, leakage and frequency dispersion of the dielectric response, which are typical for these materials[60–62]. The physical interpretation of capacitance enhancements commonly observed in ferroelectric–dielectric heterostructures[63–67] is often not straightforward, and care must be taken to rule out various artefacts, such as conductivity-induced Maxwell–Wagner effects[68,69]. Nevertheless, these studies provide strong evidence for a capacitance boost caused by the NC effect.

An important question is the nature of the NC responsible for the observed capacitance enhancement. Experimental results have often been rationalized by using the simple, single-domain model[57]; however, in most cases, depolarizing effects are expected to lead to the formation of domains. The role of domains has been explicitly addressed for $PbTiO_3/SrTiO_3$ and $Pb_{0.5}Sr_{0.5}TiO_3/SrTiO_3$ superlattices[32]. Modelling these structures as capacitors in series is complicated owing to the strong electrostatic interactions between the dielectric and ferroelectric layers[70]. However, by carefully designing the superlattices to ensure sufficient electrostatic decoupling between the ferroelectric layers, the series capacitor model can be applied, and the permittivities of the ferroelectric and dielectric layers can be separated. The NC regime can then be experimentally demonstrated over a range of temperatures, spanning both the ferroelectric and paraelectric phases (FIG. 5c)[32]. A detailed theoretical analysis combining phenomenological modelling and second-principles atomistic simulations confirmed the importance of domain wall motion and the associated changes in the interfacial

stray fields[8], but it also revealed the important role of the internal structure of the domain walls[32,33].

Device implementation. Work on ferroelectric FETs (FeFETs) has long focused on memory applications[43]; today, the idea that depolarization — one of the main foes of FeFET memory — could be exploited to improve the operation of logic devices offers an opportunity to apply the knowledge gained from studying FeFETs to NC-FETs. The subthreshold swing S, defined as the change in gate voltage V_{gate} required to change the current I_D by an order of magnitude, can be expressed as

$$S \equiv \frac{dV_{gate}}{d\log_{10}(I_D)} \equiv \underbrace{\frac{dV_{gate}}{d\phi_s}}_{m}\underbrace{\frac{d\phi_s}{d\log_{10}(I_D)}}_{n} \quad (7)$$

where φ_s is the surface potential and the transport factor $n \equiv d\phi_s/d\log_{10}(I_D)$ is set by the transport mechanism. For conventional MOSFETs, in which carriers are injected over a gate-controlled barrier, n is limited to 60 mV per decade at 300 K by Boltzmann statistics. Thus, lowering n below the Boltzmann limit requires modification of the transport mechanism, as, for example, implemented in tunnel FETs (TFETs) and impact-ionization FETs. By contrast, in NC-FETs, the body factor $m \equiv dV_{gate}/d\varphi_s$ is reduced through an amplification of φ_s by the NC effect. A major advantage of ferroelectric NC is that it can be simply integrated into existing FET structures and that it can be used in combination with approaches that decrease n to achieve further S reduction.

Experimental attempts to demonstrate steep slope operation (that is, $S < 60$ mV per decade) have focused on two approaches: direct integration of the ferroelectric into the gate stack and external connection of a ferroelectric capacitor to a FET[71–76]. In the context of NC-FETs, organic poly(vinylidenefluoride-trifluoroethylene) gate ferroelectrics[77–79] and perovskite $PbZr_{1-x}Ti_xO_3$ (PZT) gates[80,81] were explored for direct integration, whereas Aurivillius-phase $SrBi_2Ta_2O_9$ (SBT), one of the most popular choices for FeFETs and ferroelectric random-access memories, appears to have been overlooked. Although perovskite oxides can be directly grown on semiconductors[82], the unfavourable band alignment[83] and interface states at the metal–ferroelectric (M–F) interface usually require the insertion of a dielectric buffer layer, resulting in an MFIS or MFMIS stack (where I and S are the insulating buffer and semiconductor, respectively).

In the past few years, following the discovery that doped hafnia thin films exhibit ferroelectric properties, attention has rapidly shifted towards HfO_2-based materials[84–86] as NC elements. The origin of ferroelectricity in these materials is still poorly understood; however, the excellent compatibility with semiconductor-processing techniques has made HfO_2-based materials the favourite candidates for NC devices.

An important parameter in the design of NC-FETs is capacitance matching. The insulating buffer layer thickness is usually designed to optimize capacitance matching[87,88]; however, the optimization of this parameter is typically based on a model assuming homogeneous polarization, which is not valid for the multidomain case, in which the NC in the ferroelectric is approximately independent of the dielectric layer thickness above a certain value. Thus, further device modelling that explicitly considers multidomain gates with mobile domain walls is required[89,90].

The range of buffer layer materials for NC-FETs has been limited thus far, compared with the buffer layer materials explored for FeFETs[43]. The benefits and disadvantages of internal metallization in the gate stack (MFIS versus MFMIS architectures) have been discussed[41,91–94]; however, the additional MI and MF interfaces introduce additional interfacial capacitance[25,95], which has to be included in capacitance matching considerations.

In addition to devices with conventional semiconductors, other channel materials are being explored, for example, Ga_2O_3 (REF.[96]) and various 2D materials, such as MoS_2 (REFS[85,86,97]), black phosphorus[98] and WSe_2 (REF.[99]). In general, subthreshold swings substantially below 60 mV per decade have been reported for a variety of devices, which has been implicitly or explicitly attributed to static NC. However, the sharp hysteretic current–voltage curves suggest that the steep changes in current might also be associated to conventional polarization switching, as in FeFET memory devices, rather than to quasi-static NC effects.

Non-hysteretic devices tend to exhibit subthreshold swings closer to the Boltzmann limit[86–88,100,101] (FIG. 5d), although significant improvements in S over several decades in current have also been reported[102]. Unfortunately, time dependence is often not explicitly addressed, making it difficult to distinguish between transient and static effects. The investigation in REF.[86] of the effect of ramp rates for the applied bias showed that a slower ramp rate reduces the hysteresis, bringing the desired voltage amplification with subthreshold swings closer to the Boltzmann limit, suggesting that improvements in S are dominated by polarization dynamics rather than by the static NC effect[103]. Importantly, sub-60 mV per decade S is usually observed only over a limited range of gate biases, which has been attributed to difficulties in maintaining capacitance matching over the entire subthreshold region as well as in the ON state, owing to the fact that the semiconductor capacitance substantially changes from depletion to inversion. Nevertheless, recent reports of enhanced ON-state currents and transconductance in HfO_2-based FinFETs[87,88,100], as well as the improvements in short channel effects[100,101], attributed to NC operation, are very encouraging.

In summary, there is substantial evidence that integrating a ferroelectric into the gate stack can improve various transistor characteristics. However, a fundamental understanding of the precise role of NC and the types of NC involved remains elusive thus far. This requires accurate modelling approaches that simultaneously capture the electrostatics and charge dynamics within the semiconducting channel, as well as the complexities associated with ferroelectric domains and their dynamics under an applied gate bias.

Evidence for transient NC. To directly demonstrate transient NC, the voltage drop across the ferroelectric V_f must be measured during switching. One approach has

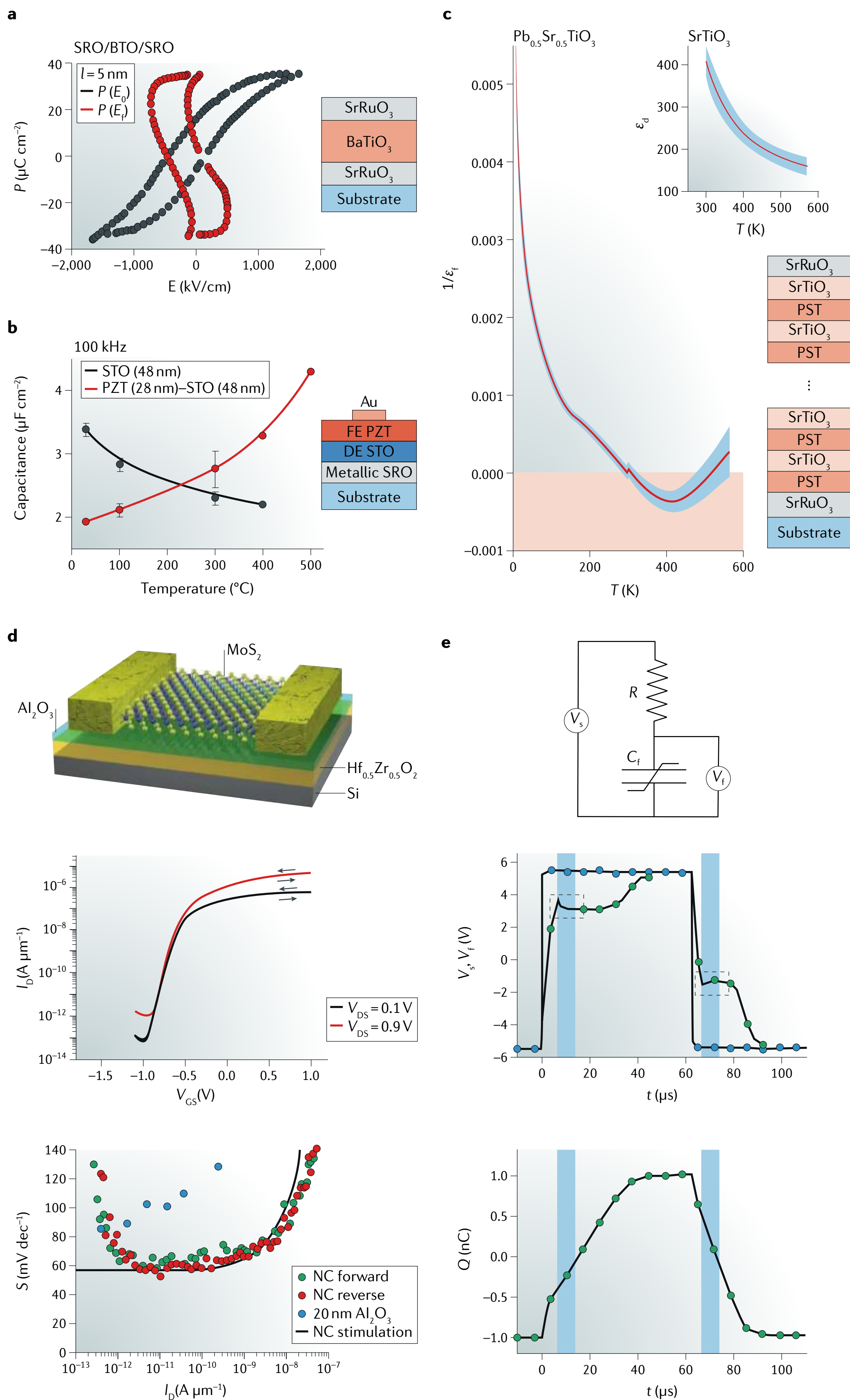
a
SRO/BTO/SRO
l = 5 nm
P (E0)
P (Ef)
P (μC cm−2)
E (kV/cm)
SrRuO3
BaTiO3
SrRuO3
Substrate
b
100 kHz
STO (48 nm)
PZT (28 nm)–STO (48 nm)
Capacitance (μF cm−2)
Temperature (°C)
Au
FE PZT
DE STO
Metallic SRO
Substrate
c
Pb0.5Sr0.5TiO3
SrTiO3
εd
T (K)
1/εf
SrRuO3
SrTiO3
PST
SrTiO3
PST
SrTiO3
PST
SrTiO3
PST
SrRuO3
Substrate
d
MoS2
Al2O3
Hf0.5Zr0.5O2
Si
ID (A μm−1)
VDS = 0.1 V
VDS = 0.9 V
VGS (V)
S (mV dec−1)
NC forward
NC reverse
20 nm Al2O3
NC stimulation
ID (A μm−1)
e
R
Vs
Cf
Vf
Vs, Vf (V)
t (μs)
Q (nC)
t (μs)

◀ Fig. 5 | **Experimental approaches to investigating negative capacitance. a** | The total voltage applied to a ferroelectric capacitor is dropped partly across the ferroelectric layer and partly across the interface capacitance that arises from the finite intrinsic screening length at the metal–ferroelectric interface. The interface capacitance can be theoretically estimated to calculate the voltage drop across the ferroelectric. Thus, the polarization P as a function of the local field in the ferroelectric E_f (red) can be obtained from the measurements of polarization as a function of the applied field E_0 (black), revealing the negative capacitance (NC) regions, as illustrated for a high-quality 5-nm-thick epitaxial $BaTiO_3$ (BTO) capacitor with $SrRuO_3$ (SRO) electrodes. **b** | A hallmark signature of NC is that capacitance is enhanced when a ferroelectric is added in series with a conventional dielectric capacitance, as shown by comparing the capacitance of an epitaxial 48-nm-thick $SrTiO_3$ (STO) capacitor with that of a bilayer capacitor consisting of 48 nm of STO and 28 nm of $PbZr_{1-x}Ti_xO_3$ (PZT). The capacitance of the bilayer exceeds that of the STO layer over a wide range of temperatures. **c** | In ferroelectric–dielectric superlattices, in which the ferroelectric layers are electrostatically decoupled owing to the formation of a dense domain structure, the ferroelectric and dielectric layers can be modelled as capacitors in series. Their effective permittivities can be separated by measuring the total capacitance of a collection of samples. For (Pb, Sr)TiO_3/$SrTiO_3$ (PST/STO) superlattices, the inverse permittivity of the ferroelectric PST layers ($1/\varepsilon_f$) displays a clear region of NC behaviour, whereas the dielectric constant of STO (ε_d) shows the typical decrease of a bulk material. **d** | An NC-field-effect transistor (FET) stack consisting of a (Hf, Zr)O_2 ferroelectric, a Al_2O_3 dielectric, a MoS_2 semiconducting channel and a doped Si gate exhibits non-hysteretic current–voltage (I_D–V_{GS}) characteristics for different values of V_{DS}, with the subthreshold swing (S) dropping below the Boltzmann limit, in contrast to the purely dielectric (Al_2O_3) gate. **e** | A typical setup for transient NC investigations consists of a ferroelectric capacitor (C_f) connected in series with a known resistance (R). The voltage across the ferroelectric capacitor (V_f, curve with green markers) and the total charge Q flowing through the circuit can be monitored as a function of time (t), following the application of a voltage pulse across the system (V_s, curve with blue markers). Regions in which dQ/dt and dV_f/dt have opposite signs (blue areas) are attributed to transient NC. D, drain; S, source. Panel **a** is adapted with permission from REF.[9], AIP Publishing. Panel **b** is adapted with permission from REF.[57], AIP Publishing. Panel **c** is adapted from REF.[32], Springer Nature Limited. Panel **d** is adapted from REF.[86], Springer Nature Limited. Panel **e** is adapted from REF.[37], Springer Nature Limited.

been to expose the internal node of an MFMIS structure and directly monitor V_f while sweeping the gate voltage across the MFMIS stack[78,104]. The resulting $P(V_f)$ hysteresis curves exhibit regions with negative slope, which were attributed to an NC effect.

Another approach is to connect a ferroelectric capacitor to an external series resistance (FIG. 5e), which slows down the delivery of charge to the capacitor plates. As a voltage across the resistor–ferroelectric circuit is applied, an NC response causes a temporary reduction in V_f, while the charge on the ferroelectric capacitor (determined by integrating the current) continues to increase[37]. Similar behaviour has been reported by many groups; however, its interpretation as a signature of the traversal of the negative $\partial Q/\partial V$ part of the ferroelectric S-shaped curve remains controversial. It is generally accepted that a realistic model should include a domain-mediated process[13] and that the observed voltage reduction originates from the mismatch between the rate at which the ferroelectric polarization switches and the delivery of the charge to the metallic plates of the capacitor[38,39]. The question remains whether the negative curvature of the free energy has to be involved in this process[37,39,46–48]. A variant of this direct method to monitor transient NC is to replace the series resistor with an external series capacitance[105]; the capacitor then directly controls the charge on the ferroelectric, as originally proposed by Salahuddin and Datta[10].

Perspectives

Decades after the pioneering works of Landauer, Bratkovsky and Levanyuk and the visionary article of Salahuddin and Datta[7–10], the field of ferroelectric NC is now gaining momentum, driven by progress in low-power transistor technology and, particularly, by the development of hafnia-related ferroelectric materials that can be readily grown on semiconductors. All expected behaviours associated with NC (in particular, capacitance enhancement and voltage amplification) have been repeatedly experimentally reported, supporting the existence of a local NC response. The essential features of the NC effect are now also theoretically understood, even for the most challenging (and typical) case of a ferroelectric in the multidomain state. Furthermore, first-principles atomistic simulations can reproduce and explain NC behaviours in realistic situations, notably in ferroelectric–dielectric superlattices. However, many challenges remain to provide a thorough understanding of NC behaviour and to optimize the intrinsic NC response.

An important issue is the enhancement of the NC response, that is, C_f^{-1} needs to be as negative as possible to maximize voltage amplification. Moreover, the temperature range of the NC region needs to be extended. The NC response can be enhanced by pushing down $T_{\uparrow\downarrow}$ (the temperature for the onset of the multidomain ferroelectric state), to separate it from T_0 (the nominal transition temperature) and bring it as close as possible to $T_{\uparrow\uparrow}$ (the temperature at which the monodomain ferroelectric state appears) (FIG. 2). This strategy can be used to increase the incipient ferroelectric region ($T_{\uparrow\downarrow} < T < T_0$) and approach $T_{\uparrow\uparrow}$, at which the largest NC responses are expected[22]. The distance between $T_{\uparrow\downarrow}$ and T_0 increases with domain wall formation energy, and thus ferroelectric materials with unfavourable domain walls would be ideal to obtain a large NC response of an incipient ferroelectric type. Therefore, ferroelectrics with high domain wall energy can be expected to play an important role in the context of NC optimization.

Domain wall mobility and large polarizability further play a key role in the NC response of a multidomain state. For example, in $PbTiO_3$/$SrTiO_3$ superlattices[32,33], domain wall mobility and large polarizability are crucial to obtain a net $C_f < 0$ in the ferroelectric layers. Furthermore, in nanoscale ferroelectrics, domain walls can be very wide[29] (comparable to the size of the domains) and have a complex structure[106]. Thus, by controlling the structure and properties of the walls, it may be possible to enhance the NC response. For example, the walls could present some sort of incipient order that could contribute to an NC response (this might be the case for the domain walls in $PbTiO_3$ (REF.[107])). Moreover, inducing attractive wall–wall interactions that go beyond electrostatic effects should result in a greater inhomogeneous enhancement of the NC response (smaller κ, in equation 5) and a stronger NC effect.

Importantly, the $C_f < 0$ behaviour is made possible — as well as controlled and limited — by the parts in contact with the ferroelectric material. Thus, these parts and the corresponding interfaces with the ferroelectric have an impact on C_f. For example, by using a dielectric

with a strong nonlinear response, $dC_s/dE < 0$, the range of negative C_f values compatible with global thermodynamic stability ($C > 0$) can be expanded, enabling an optimized NC behaviour. Similarly, chemical effects (for example, the formation of new bonds or new structures) at the interfaces between ferroelectrics and other materials may impact the polar instabilities and associated responses[95], which offers another possibility to tune NC. Indeed, the NC response is not a property of only the ferroelectric material, and thus optimization strategies do not have to be limited to the ferroelectric.

The specific application or device also needs to be considered, because it determines the environment of the ferroelectric and its response. FETs are currently the most interesting and best-studied case, and the impact of various design variables (size, shape, response and conductivity of the different components) on the voltage amplification effect is being intensively investigated, including by dynamic simulation studies[20,51,71,93,94,108–118]. Applying NC effects in transistors is challenging owing to the presence of free carriers in the channel, which is in contact with the source and drain, complicating the realization of charge-control conditions as well as the stabilization of the NC state. Thus, in the context of FET applications, optimization of the NC effects is strongly influenced (and limited) by the behaviour of the carriers in the semiconducting channel.

An important yet underrated topic is the dynamical electromagnetic response of domain structures in ferroelectrics with NC. Theory predicts a distinct resonance behaviour at sub-terahertz frequencies, once the real part of the dynamical permittivity changes its sign from negative (at low frequencies) to positive (at high frequencies)[30]. This effect is very similar to plasma UV resonance in metals but occurs in the sub-terahertz frequency range, which is the desired range for nanoelectronic and plasmonic applications to process ultrafast signals. Interestingly, at the frequency at which the permittivity crosses zero, the refractive index must change from complex to real[30] — a remarkable effect that has not yet been experimentally studied.

Finally, let us comment on the different families of ferroelectric materials used in NC studies and applications. Initially, polymeric and perovskite-oxide ferroelectrics were predominantly explored. However, hafnia-based compounds[18] have key technological advantages, making this material an important player in future applications of ferroelectricity in electronics. The behaviour of ferroelectric hafnia is not yet fully understood or characterized, but hafnia-based ferroelectrics exhibit interesting properties. For example, in HfO_2-related compounds, the polar instability does not manifest itself as obviously as in other ferroelectrics (for example, in giant electromechanical responses). Hafnia further displays properties different from those of other ferroelectric materials, such as a pronounced polymorphism and the existence of competing anti-ferroelectric and amorphous phases. These distinct features might be of interest in the context of NC applications, because they may allow additional possibilities for tuning or optimizing the response of the ferroelectric.

Therefore, well-known compounds, such as ferroelectrics based on $PbTiO_3$ or $BaTiO_3$, offer NC optimization possibilities (for example, based on their soft-mode response) that may be impossible in HfO_2-based materials and continue to deserve our attention. Regarding NC optimization in hafnia-based materials, taking advantage of their specific features and behaviours will require a deeper understanding of their ferroelectric and dielectric properties.

Published online 14 March 2019

1. Landau, L. & Lifshitz, E. *Electrodynamics of Continuous Media* (Pergamon, 1960).
2. Verman, L. C. Negative circuit constants. *Proc. Inst. Radio Eng.* **19**, 676–681 (1931).
3. Behr, L. & Tarpley, R. Design of resistors for precise high-frequency measurements. *Proc. Inst. Radio Eng.* **20**, 1101–1113 (1932).
4. Terman, F. E. Variable reactance circuit. US Patent 1950759 (1934).
5. Harty, J. The influence of depolarizers upon the photovoltaic effect in cells containing grignard reagents. *J. Phys. Chem.* **39**, 355–370 (1935).
6. Bening, F. *Negative Widerstände in Elektronischen Schaltungen* (Verlag Technik, 1971).
7. Landauer, R. Can capacitance be negative? *Collect. Phenom.* **2**, 167–170 (1976).
8. Bratkovsky, A. M. & Levanyuk, A. P. Very large dielectric response of thin ferroelectric films with the dead layers. *Phys. Rev. B* **63**, 2–5 (2001).
9. Bratkovsky, A. M. & Levanyuk, A. P. Depolarizing field and "real" hysteresis loops in nanometer-scale ferroelectric films. *Appl. Phys. Lett.* **89**, 253108 (2006).
10. Salahuddin, S. & Datta, S. Use of negative capacitance to provide voltage amplification for low power nanoscale devices. *Nano Lett.* **8**, 405–410 (2008).
11. Zhirnov, V. V. & Cavin, R. K. Nanoelectronics: negative capacitance to the rescue? *Nat. Nanotechnol.* **3**, 77–78 (2008).
12. Theis, T. N. & Solomon, P. M. It's time to reinvent the transistor! *Science* **327**, 1600–1601 (2010).
13. Catalan, G., Jiménez, D. & Gruverman, A. Ferroelectrics: negative capacitance detected. *Nat. Mater.* **14**, 137–139 (2015).
14. Ionescu, A. M. Negative capacitance gives a positive boost. *Nat. Nanotechnol.* **13**, 7–8 (2018).
15. Boescke, T. S. et al. Phase transitions in ferroelectric silicon doped hafnium oxide. *Appl. Phys. Lett.* **99**, 112904 (2011).
16. Müller, J. et al. Ferroelectricity in simple binary ZrO_2 and HfO_2. *Nano Lett.* **12**, 4318–4323 (2012).
17. Mueller, S. et al. Incipient ferroelectricity in Al-doped HfO_2 thin films. *Adv. Funct. Mater.* **22**, 2412–2417 (2012).
18. Park, M. H. et al. Ferroelectricity and antiferroelectricity of doped thin HfO_2-based films. *Adv. Mater.* **27**, 1811–1831 (2015).
19. Abele, N. et al. Suspended-gate mosfet: bringing new mems functionality into solid-state mos transistor. Presented at the 2005 *IEEE International Electron Devices Meeting* (2005).
20. Jain, A. & Alam, M. A. Stability constraints define the minimum subthreshold swing of a negative capacitance field-effect transistor. *IEEE Trans. Electron Devices* **61**, 2235–2242 (2014).
21. Li, L. et al. Very large capacitance enhancement in a two-dimensional electron system. *Science* **332**, 825–828 (2011).
22. Cano, A. & Jiménez, D. Multidomain ferroelectricity as a limiting factor for voltage amplification in ferroelectric field-effect transistors. *Appl. Phys. Lett.* **97**, 10–12 (2010).
23. Mehta, R. R., Silverman, B. D. & Jacobs, J. T. Depolarization fields in thin ferroelectric films. *J. Appl. Phys.* **44**, 3379–3385 (1973).
24. Junquera, J. & Ghosez, P. Critical thickness for ferroelectricity in perovskite ultrathin films. *Nature* **422**, 506–509 (2003).
25. Stengel, M. & Spaldin, N. A. Origin of the dielectric dead layer in nanoscale capacitors. *Nature* **443**, 679–682 (2006).
26. Neaton, J. B. & Rabe, K. M. Theory of polarization enhancement in epitaxial $BaTiO_3/SrTiO_3$ superlattices. *Appl. Phys. Lett.* **82**, 1586–1588 (2003).
27. Dawber, M. et al. Tailoring the properties of artificially layered ferroelectric superlattices. *Adv. Mater.* **19**, 4153 (2007).
28. Saeidi, A. et al. Negative capacitance field effect transistors; capacitance matching and non-hysteretic operation. Presented at the *47th European Solid-State Device Research Conference (ESSDERC)* (2017).
29. De Guerville, F., Luk'yanchuk, I., Lahoche, L. & El Marssi, M. Modeling of ferroelectric domains in thin films and superlattices. *Mater. Sci. Eng. B* **120**, 16–20 (2005).
30. Luk'yanchuk, I., Sené, A. & Vinokur, V. M. Electrodynamics of ferroelectric films with negative capacitance. *Phys. Rev. B* **98**, 024107 (2018).
31. Íñiguez et al. General theory of ferroelectric negative capacitance. In the press (2019).
32. Zubko, P. et al. Negative capacitance in multidomain ferroelectric superlattices. *Nature* **534**, 524–528 (2016).
33. Yadav, A. K. et al. Spatially resolved steady-state negative capacitance. *Nature* **565**, 468–471 (2019).
34. Ponomareva, I., Bellaiche, L. & Resta, R. Dielectric anomalies in ferroelectric nanostructures. *Phys. Rev. Lett.* **99**, 227601 (2007).
35. Luk'yanchuk, I., Tikhonov, Y., Sené, A., Razumnaya, A. & Vinokur, V. M. Harnessing ferroelectric domains for negative capacitance. *Commun. Phys.* **2**, 22 (2019).
36. Ricinschi, D. et al. Analysis of ferroelectric switching in finite media as a landau-type phase transition. *J. Phys. Condens. Matter* **10**, 477 (1998).

37. Khan, A. I. et al. Negative capacitance in a ferroelectric capacitor. *Nat. Mater.* **14**, 182–186 (2015).
38. Ng, K., Hillenius, S. J. & Gruverman, A. Transient nature of negative capacitance in ferroelectric field-effect transistors. *Solid State Commun.* **265**, 12–14 (2017).
39. Chang, S.-C., Avci, U. E., Nikonov, D. E., Manipatruni, S. & Young, I. A. Physical origin of transient negative capacitance in a ferroelectric capacitor. *Phys. Rev. Appl.* **9**, 014010 (2018).
40. Hoffmann, M. et al. Ferroelectric negative capacitance domain dynamics. *J. Appl. Phys.* **123**, 184101 (2018).
41. Hoffmann, M., Pesic, M., Slesazeck, S., Schroeder, U. & Mikolajick, T. On the stabilization of ferroelectric negative capacitance in nanoscale devices. *Nanoscale* **10**, 10891–10899 (2018).
42. Ducharme, S. et al. Intrinsic ferroelectric coercive field. *Phys. Rev. Lett.* **84**, 175–178 (2000).
43. Dawber, M., Rabe, K. M. & Scott, J. F. Physics of thin-film ferroelectric oxides. *Rev. Mod. Phys.* **77**, 1083–1130 (2005).
44. Highland, M. J. et al. Polarization switching without domain formation at the intrinsic coercive field in ultrathin ferroelectric $PbTiO_3$. *Phys. Rev. Lett.* **105**, 167601 (2010).
45. Mankowsky, R., von Hoegen, A., Först, M. & Cavalleri, A. Ultrafast reversal of the ferroelectric polarization. *Phys. Rev. Lett.* **118**, 197601 (2017).
46. Song, S. J. et al. Alternative interpretations for decreasing voltage with increasing charge in ferroelectric capacitors. *Sci. Rep.* **6**, 1–6 (2016).
47. Kim, Y. J. et al. Voltage drop in a ferroelectric single layer capacitor by retarded domain nucleation. *Nano Lett.* **17**, 7796–7802 (2017).
48. Saha, A. K., Datta, S. & Gupta, S. K. “Negative capacitance” in resistor-ferroelectric and ferroelectric-dielectric networks: apparent or intrinsic? *J. Appl. Phys.* **123**, 105102 (2018).
49. Sluka, T., Mokry, P. & Setter, N. Static negative capacitance of a ferroelectric nano-domain nucleus. *Appl. Phys. Lett.* **111**, 152902 (2017).
50. Saha, A., Sharma, P., Dabo, I., Datta, S. & Gupta, S. Ferroelectric transistor model based on self-consistent solution of 2d poisson’s, non-equilibrium green’s function and multi-domain landau khalatnikov equations. *Presented at the 2017 Electron Devices Meeting (IEDM)* (2017).
51. Smith, S., Chatterjee, K. & Salahuddin, S. Multidomain phase-field modeling of negative capacitance switching transients. *IEEE Trans. Electron Devices* **65**, 295–298 (2017).
52. Hoffmann, M. et al. Ferroelectric negative capacitance domain dynamics. *Appl. Phys. Rev.* **123**, 184101 (2018).
53. Jonscher, A. K. The physical origin of negative capacitance. *J. Chem. Soc. Faraday Trans. 2* **82**, 75 (1986).
54. Ershov, M. et al. Negative capacitance effect in semiconductor devices. *IEEE Trans. Electron Devices* **45**, 2196–2206 (1998).
55. Kim, D. J. et al. Polarization relaxation induced by a depolarization field in ultrathin ferroelectric $BaTiO_3$ capacitors. *Phys. Rev. Lett.* **95**, 237602 (2005).
56. Zubko, P. et al. On the persistence of polar domains in ultrathin ferroelectric capacitors. *J. Phys.: Condens. Matter* **29**, 284001 (2017).
57. Islam Khan, A. et al. Experimental evidence of ferroelectric negative capacitance in nanoscale heterostructures. *Appl. Phys. Lett.* **99**, 113501 (2011).
58. Appleby, D. J. R. et al. Experimental observation of negative capacitance in ferroelectrics at room temperature. *Nano Lett.* **14**, 3864–3868 (2014).
59. Gao, W. et al. Room-temperature negative capacitance in a ferroelectric-dielectric superlattice heterostructure. *Nano Lett.* **14**, 5814–5819 (2014).
60. Kim, Y. J. et al. Frustration of negative capacitance in $Al_2O_3/BaTiO_3$ bilayer structure. *Sci. Rep.* **6**, 19039 (2016).
61. Kim, Y. J. et al. Time-dependent negative capacitance effects in $Al_2O_3/BaTiO_3$ bilayers. *Nano Lett.* **16**, 4375–4381 (2016).
62. Rusu, A., Saeidi, A. & Ionescu, A. M. Condition for the negative capacitance effect in metal–ferroelectric–insulator–semiconductor devices. *Nanotechnology* **27**, 115201 (2016).
63. Tabata, H., Tanaka, H. & Kawai, T. Formation of artificial $BaTiO_3/SrTiO_3$ superlattices using pulsed laser deposition and their dielectric properties. *Appl. Phys. Lett.* **65**, 1970–1972 (1994).
64. Erbil, A., Kim, Y. & Gerhardt, R. A. Giant permittivity in epitaxial ferroelectric heterostructures. *Phys. Rev. Lett.* **77**, 1628–1631 (1996).
65. Corbett, M. H., Bowman, R. M., Gregg, J. M. & Foord, D. T. Enhancement of dielectric constant and associated coupling of polarization behavior in thin film relaxor superlattices. *Appl. Phys. Lett.* **79**, 815–817 (2001).
66. Park, J. D. & Oh, T. S. Characteristics of $Pt/SBT/ZrO_2/Si$ structure for metal ferroelectric insulator semiconductor field effect transistor applications. *Integr. Ferroelectr.* **34**, 121–130 (2001).
67. Kim, L., Jung, D., Kim, J., Kim, Y. S. & Lee, J. Strain manipulation in $BaTiO_3/SrTiO_3$ artificial lattice toward high dielectric constant and its nonlinearity. *Appl. Phys. Lett.* **82**, 2118–2120 (2003).
68. Catalan, G., O’Neill, D., Bowman, R. M. & Gregg, J. M. Relaxor features in ferroelectric superlattices: a Maxwell–Wagner approach. *Appl. Phys. Lett.* **77**, 3078–3080 (2000).
69. O’Neill, D., Bowman, R. M. & Gregg, J. M. Dielectric enhancement and Maxwell–Wagner effects in ferroelectric superlattice structures. *Appl. Phys. Lett.* **77**, 1520–1522 (2000).
70. Sun, F.-C., Kesim, M. T., Espinal, Y. & Alpay, S. P. Are ferroelectric multilayers capacitors in series? *J. Mater. Sci.* **51**, 499–505 (2016).
71. Khan, A. I. et al. Negative capacitance in short-channel FinFETs externally connected to an epitaxial ferroelectric capacitor. *IEEE Electron Device Lett.* **37**, 111–114 (2016).
72. Jo, J. et al. Negative capacitance in organic/ferroelectric capacitor to implement steep switching MOSdevices. *Nano Lett.* **15**, 4553–4556 (2015).
73. Jo, J. & Shin, C. Negative capacitance field effect transistor with hysteresis-free sub-60-mV/decade switching. *IEEE Electron Device Lett.* **37**, 245–248 (2016).
74. Ko, E., Lee, H., Goh, Y., Jeon, S. & Shin, C. Sub-60-mV/decade negative capacitance FinFET with sub-10-nm hafnium-based. *IEEE J. Electron Devices Soc.* **5**, 10–13 (2017).
75. Saeidi, A. et al. Negative capacitance as performance booster for tunnel FETs and MOSFETs: an experimental study. *IEEE Electron Device Lett.* **38**, 1485–1488 (2017).
76. Saedi, S. et al. Effect of hysteretic and non-hysteretic negative capacitance on tunnel FETs DC performance. *Nanotechnology* **29**, 095202 (2018).
77. Salvatore, G. A., Bouvet, D. & Ionescu, A. M. Demonstration of subthrehold swing smaller than 60 mV/decade in Fe-FET with P(VDF-TrFE)/SiO_2 gate stack. Presented at the *2008 IEEE International Electron Devices Meeting* (2008).
78. Rusu, A., Salvatore, G. A., Jimenez, D. & Ionescu, A. M. Metal-ferroelectric-metal-oxide-semiconductor field effect transistor with sub-60 mV/decade subthreshold swing and internal voltage amplification. Presented at the *2010 International Electron Devices Meeting* (2010).
79. Salvatore, G. A. et al. Ferroelectric transistors with improved characteristics at high temperature. *Appl. Phys. Lett.* **97**, 053503 (2010).
80. Dasgupta, S. et al. Sub-kT/q switching in strong inversion in $PbZr_{0.52}Ti_{0.48}O_3$-gated negative capacitance FETs. *IEEE J. Explor. Solid State Comput. Devices Circuits* **1**, 43–48 (2015).
81. Park, J. H. et al. Sub-kT/q subthreshold-slope using negative capacitance in low-temperature polycrystalline-silicon thin-film transistor. *Sci. Rep.*.**6**, 24734 (2016).
82. Mazet, L., Yang, S. M., Kalinin, S. V., Schamm-Chardon, S. & Dubourdieu, C. A review of molecular beam epitaxy of ferroelectric $BaTiO_3$ films on Si, Ge and GaAs substrates and their applications. *Sci. Technol. Adv. Mater.* **16**, 036005 (2015).
83. Robertson, J. & Chen, C. W. Schottky barrier heights of tantalum oxide, barium strontium titanate, lead titanate, and strontium bismuth tantalate. *Appl. Phys. Lett.* **74**, 1168–1170 (1999).
84. Cheng, C. H. & Chin, A. Low-voltage steep turn-on pMOSFET using ferroelectric high-κ gate dielectric. *IEEE Electron Device Lett.* **35**, 274–276 (2014).
85. McGuire, F. A. et al. Sustained sub-60 mV/decade switching via the negative capacitance effect in MoS_2 transistors. *Nano Lett.* **17**, 4801–4806 (2017).
86. Si, M. et al. Steep-slope hysteresis-free negative capacitance MoS_2 transistors. *Nat. Nanotechnol.* **2017**, 1 (2017).
87. Krivokapic, Z. et al. 14 nm ferroelectric finfet technology with steep subthreshold slope for ultra low power applications. Presented at the *2017 IEEE International Electron Devices Meeting (IEDM)* (2017).
88. Krivokapic, Z. et al. Ncfet: opportunities & challenges for advanced technology nodes. Presented at the *2017 Fifth Berkeley Symposium on Energy Efficient Electronic Systems Steep Transistors Workshop (E3S)* (2017).
89. Misirlioglu, I. B., Yildiz, M. & Sendur, K. Domain control of carrier density at a semiconductor-ferroelectric interface. *Sci. Rep.* **5**, 14740 (2015).
90. Misirlioglu, I. B., Sen, C., Kesim, M. T. & Alpay, S. P. Low-voltage ferroelectric-paraelectric superlattices as gate materials for field-effect transistors. *J. Mater. Sci.* **51**, 487–498 (2016).
91. Frank, D. J. et al. The quantum metal ferroelectric field-effect transistor. *IEEE Trans. Electron Devices* **61**, 2145–2153 (2014).
92. Khan, A. I., Radhakrishna, U., Chatterjee, K., Salahuddin, S. & Antoniadis, D. A. Negative capacitance behavior in a leaky ferroelectric. *IEEE Trans. Electron Devices* **63**, 4416–4422 (2016).
93. Duarte, J. P. et al. Compact models of negative-capacitance finfets: lumped and distributed charge models. Presented at the *2016 IEEE International Electron Devices Meeting (IEDM)* (2016).
94. Pahwa, G., Dutta, T., Agarwal, A. & Chauhan, Y. S. Physical insights on negative capacitance transistors in nonhysteresis and hysteresis regimes: MFMIS versus MFIS structures. *IEEE Trans. Electron Devices* **65**, 867–873 (2018).
95. Stengel, M., Vanderbilt, D. & Spaldin, N. A. Enhancement of ferroelectricity at metal–oxide interfaces. *Nat. Mater.* **8**, 392 (2009).
96. Si, M., Yang, L., Zhou, H. & Ye, P. D. β-Ga_2O_3 nanomembrane negative capacitance field-effect transistors with steep subthreshold slope for wide band gap logic applications. *ACS Omega* **2**, 7136–7140 (2017).
97. McGuire, F. A., Cheng, Z., Price, K. & Franklin, A. D. Sub-60 mV/decade switching in 2D negative capacitance field-effect transistors with integrated ferroelectric polymer. *Appl. Phys. Lett.* **109**, 093101 (2016).
98. Liu, F. et al. Negative capacitance transistors with monolayer black phosphorus. *NPJ Quantum Mater.* **1**, 16004 (2016).
99. Si, M. et al. Steep-slope WSe_2 negative capacitance field-effect transistor. *Nanoletters* **18**, 3682–3687 (2018).
100. Zhou, H. et al. Negative capacitance, n-channel, Si FinFETs: bi-directional sub-60 mV/dec, negative DIBL, negative differential resistance and improved short channel effect. Presented at the *2018 IEEE Symposium on VLSI Technology* (2018).
101. Kwon, D. et al. Improved subthreshold swing and short channel effect in FDSOI n-channel negative capacitance field effect transistors. *IEEE Electron Device Lett.* **39**, 300–303 (2018).
102. Yu, Z. et al. Negative capacitance 2D MoS_2 transistors with sub-60 mV/dec subthreshold swing over 6 orders, 250 μA/μm current density, and nearly-hysteresis-free. Presented at the *2017 IEEE International Electron Devices Meeting (IEDM)* (2017).
103. Houdt, J. V. & Roussel, P. Physical model for the steep subthreshold slope in ferroelectric FETs. *IEEE Electron Device Lett.* **39**, 877–880 (2018).
104. Salvatore, G. A., Rusu, A. & Ionescu, A. M. Experimental confirmation of temperature dependent negative capacitance in ferroelectric field effect transistor. *Appl. Phys. Lett.* **100**, 163504 (2012).
105. Khan, A. I. et al. Differential voltage amplification from ferroelectric negative capacitance. *Appl. Phys. Lett.* **111**, 253501 (2017).
106. Yadav, A. K. et al. Observation of polar vortices in oxide superlattices. *Nature* **530**, 198–201 (2016).
107. Wojdeł, J. C. & Íñiguez, J. Ferroelectric transitions at ferroelectric domain walls found from first principles. *Phys. Rev. Lett.* **112**, 247603 (2014).
108. Jimenez, D., Miranda, E. & Godoy, A. Analytic model for the surface potential and drain current in negative capacitance field-effect transistors. *IEEE Trans. Electron Devices* **57**, 2405–2409 (2010).
109. Xiao, Y. et al. Simulation of electrical characteristics in negative capacitance surrounding-gate ferroelectric field-effect transistors. *Appl. Phys. Lett.* **101**, 253511 (2012).
110. Yuan, Z. C. et al. Switching-speed limitations of ferroelectric negative-capacitance FETs. *IEEE Trans. Electron Devices* **63**, 4046–4052 (2016).
111. Jiang, C., Liang, R., Wang, J. & Xu, J. Simulation-based study of negative capacitance double-gate

junctionless transistors with ferroelectric gate dielectric. *Solid State Electron.* **126**, 130–135 (2016).
112. Lin, C.-I., Khan, A. I., Salahuddin, S. & Hu, C. Effects of the variation of ferroelectric properties on negative capacitance FET characteristics. *IEEE Trans. Electron Devices* **63**, 2197 (2016).
113. Aziz, A., Ghosh, S. G., Datta, S. & Gupta, S. K. Physics-based circuit-compatible spice model for ferroelectric transistors. *IEEE Electron. Device Lett.* **37**, 805 (2016).
114. Li, Y., Kang, Y. & Gong, X. Evaluation of negative capacitance ferroelectric MOSFET for analog circuit applications. *IEEE Trans. Electron Devices* **64**, 4317–4321 (2017).
115. Pahwa, G., Dutta, T., Agarwal, A. & Chauhan, Y. S. Compact model for ferroelectric negative capacitance transistor with MFIS structure. *IEEE Trans. Electron Devices* **64**, 1366–1374 (2017).
116. Chatterjee, K., Rosner, A. J. & Salahuddin, S. Intrinsic speed limit of negative capacitance transistors. *IEEE Electron Device Lett.* **38**, 1328–1330 (2017).
117. Rasool, R., Rather, G. & ud-Din, N. Analytic model for the electrical properties of negative capacitance metal-ferroelectric insulator silicon (MFIS) capacitor. *Integr. Ferroelectr.* **185**, 93–101 (2017).
118. Zhang, X., Lam, K.-T., Low, K. L., Yeo, Y.-C. & Liang, G. Nanoscale fets simulation based on full-complex-band structure and self-consistently solved atomic potential. *IEEE Trans. Electron Devices* **64**, 58–65 (2017).

Acknowledgements

For useful feedback and illuminating discussions, the authors thank L. Bellaiche, E. Defay, P. Garcia-Fernández, D. Jiménez, S. Salahuddin, J. F. Scott and M. Stengel. The work was funded by the Luxembourg National Research Fund (grant FNR/C15/MS/10458889 "NEWALLS", J.Í.), the UK Engineering and Physical Sciences Research Council (EPSRC) (grant EP/M007073/1, P.Z.), the European Commission (grant ENGIMA-H2020-MSCA-RISE-2017, I.L.) and ETH-Zurich (A.C.). Finally, a good part of this Review was completed during TOPO2018, the International Workshop on Topological Structures in Ferroic Materials, sponsored and hosted by the International Institute of Physics (IIP) of the Federal University of Rio Grande do Norte (UFRN) (Natal, Brazil); the authors are grateful to the IIP for the hospitality and excellent work atmosphere.

Author contributions

All authors contributed equally to this article.

Competing interests

The authors declare no competing interests.

Publisher's note

Springer Nature remains neutral with regard to jurisdictional claims in published maps and institutional affiliations.